A hierarchical knowledge-based classification for glacier terrain mapping: a case study from Kolahoi Glacier, Kashmir Himalaya

Aparna SHUKLA,[1] Iram ALI[2]

[1]Wadia Institute of Himalayan Geology (WIHG), Dehradun, India
[2]Department of Earth Sciences, University of Kashmir, Srinagar, India
Correspondence: Aparna Shukla <aparna.shukla22@gmail.com>

ABSTRACT. A glacierized terrain comprises different land covers, and their mapping using satellite data is challenged by their spectral similarity. We propose a hierarchical knowledge-based classification (HKBC) approach for differentiation of glacier terrain classes and mapping of glacier boundaries, using Advanced Spaceborne Thermal Emission and Reflection Radiometer (ASTER) imagery and Global Digital Elevation Model (GDEM). The methodology was tested over Kolahoi Glacier, Kashmir Himalaya. For the sequential extraction of various glacier terrain classes, several input layers were generated from the primary datasets by applying image-processing techniques. Noticeable differences in temperature and spectral response between supraglacial debris and periglacial debris facilitated the development of a thermal glacier mask and normalized-difference debris index, which together with slope enabled their differentiation. These and the other layers were then used in several discrete tests in HKBC, to map various glacier terrain classes. An ASTER visible near-infrared image and 42 field points were used to validate results. The proposed approach satisfactorily classified all the glacier terrain classes with an overall accuracy of 89%. The Z-test reveals that results obtained from HKBC are significantly (at 95% confidence level) better than those from a maximum likelihood classifier (MLC). Glacier boundaries obtained from HKBC were found to be plausibly better than those obtained from MLC and visual interpretation.

KEYWORDS: debris-covered glaciers, glacier delineation, glacier mapping, supraglacial debris

INTRODUCTION

As an integral part of the cryosphere, mountain glaciers constitute one of the most important components of the Earth's natural system and serve as sensitive climate-change indicators (Scherler and others, 2011). Therefore, their accurate mapping and monitoring are of vital importance for the proper planning and management of water resources. Considering the extent and inaccessibility of glaciers, remote sensing acts as an effective technology for their regular mapping in a comprehensive and effective manner (Bolch and others, 2010; Bhambri and others, 2011; Paul and Mölg, 2014). Precise areal extents of various glacier terrain classes are directly or indirectly used in various studies. Different snow-ice classes (e.g. dry snow, wet snow, ice, ice-mixed debris) have different water storage capacity, and changes or inter-conversions between them greatly influence the storage of glaciers (Jansson and others, 2003). Dry and wet snow areas are important for avalanche vulnerability assessment. Differentiation of snow and ice also facilitates mass-balance estimates based on observations of the accumulation–area ratio. Thus, accurate mapping of these classes would greatly influence the precision of hydrological modelling, avalanche prediction/forecasting models and glacier mass-balance studies. Also, correct quantification of the areal extents of the supraglacial debris and its temporal variations may give a clear indication of the glacier's health (Shukla and others, 2009; Racoviteanu and Williams, 2012; Reid and Brock, 2014).

Techniques for glacier-cover mapping include (1) band ratio techniques (Kääb, 2002; Paul and others, 2013); (2) image classification techniques based on spectral indices (Keshri and others, 2009; Burns and Nolin, 2014; Bhardwaj and others, 2015); (3) morphometric analysis of attributes such as slope, aspect and elevation (Bolch and others, 2007; Shukla and others, 2010a); (4) multi-source and texture analysis (Paul and others, 2004; Racoviteanu and Williams, 2012); and (5) supervised classification (Bayr and others, 1994; Shukla and others, 2009; Khan and others, 2015). These research methodologies have mapped glacier facies with varying success and have been effective in distinguishing debris-free glacier ice from debris cover, but report difficulties in separating debris on the glacier surface from surrounding terrain (Shukla and others, 2010a,b; Racoviteanu and Williams, 2012). Debris may be present either on the surface of the glacier, called supraglacial debris (SGD), or along the margins of the glacier, called periglacial debris (PGD) (Shukla and others, 2010a). In the ablation zone, towards the glacier terminus, as ice starts giving way to supraglacial debris, there forms a mixture of the two classes called ice-mixed debris (IMD) (Keshri and others, 2009), also sometimes referred to as 'dirty glacier ice' or 'mixed ice' (Bhardwaj and others, 2015). This mixed class covers a region between the total ice-covered area in the upper reaches of the ablation zone and the total debris-covered area in the lower reaches of the ablation zone, i.e. the glacier snout. Both SGD and PGD originate from surrounding valley rock, and are indistinguishable on multispectral satellite images. Thus, they act as a major constraint on accurate satellite-based mapping of glaciers (Paul and others, 2004, 2013; Shukla and others, 2010a). Differentiation of SGD and PGD classes can facilitate automatic glacier mapping (Shukla and others, 2010a,b).
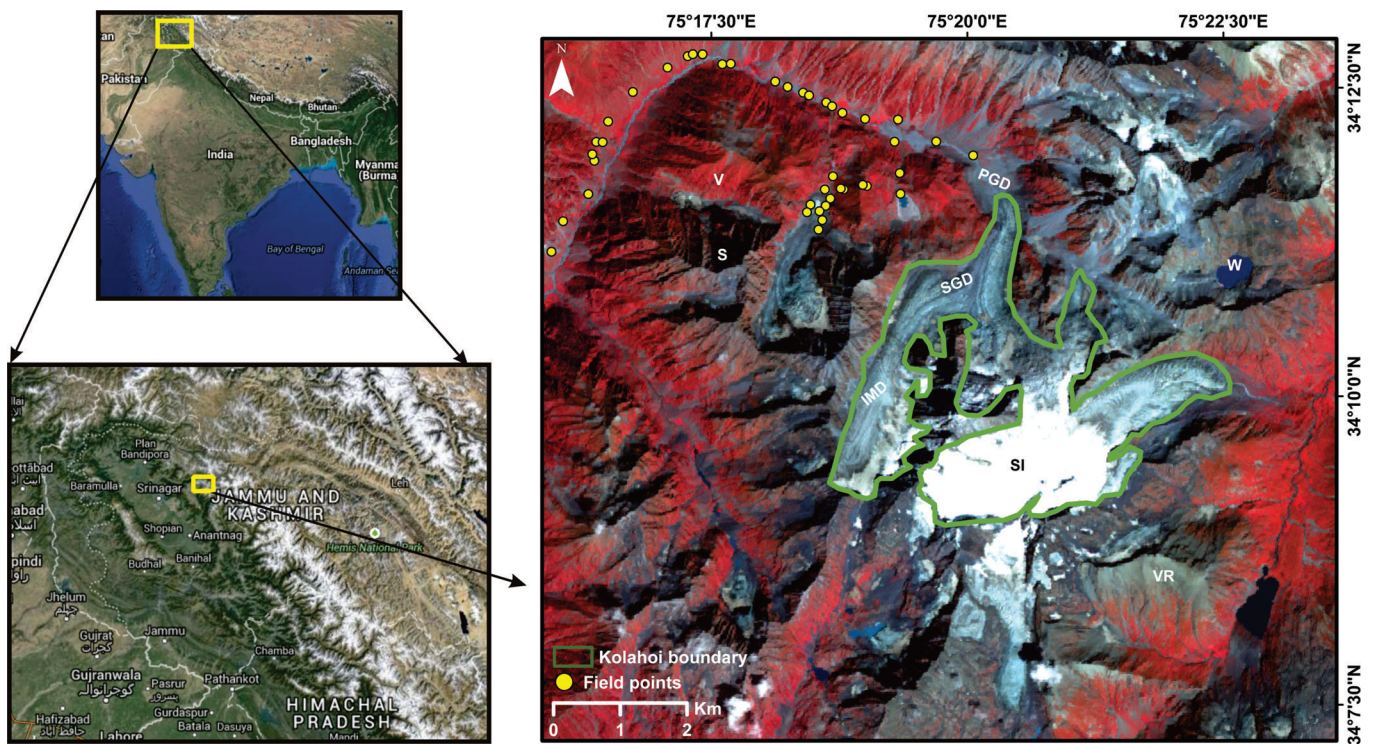
Fig. 1. The ASTER false-colour composite on the right shows Kolahoi Glacier and the adjoining area, with band combination R = near infrared, G = red and B = green band. In this map the abbreviations are W: water; V: vegetation; SI: snow-ice; S: shadow; IMD: ice-mixed debris; SGD: supraglacial debris; PGD: periglacial debris; VR: valley rock. Circles represent the set of field-based observations collected during September 2014. Zoomed-out images on left show location of the study site within the region (bottom) and of the region within the subcontinent (top).

Many works have reported this problem and have proposed improved techniques for mapping the margins of glaciers with varying amounts of debris cover in the ablation area.

A literature review suggests that optical data alone are insufficient for mapping glacier margins, especially when they are covered with varying amounts of debris. Previous studies have shown that inputs from other sources such as geomorphometry (Bolch and Kamp, 2006), thermal data (Ranzi and others, 2004) or a combination of these (Paul and others, 2004; Bolch and other, 2008; Shukla and others, 2010a,b; Bhambri and others, 2012; Karimi and others, 2012; Tiwari and others, in press) are needed together with optical data for effective mapping of glacier margins. Recently Bhardwaj and others (2015) demonstrated a Landsat 8 Operational Land Imager sensor based algorithm for automated mapping of glacier facies and supraglacial debris. This method used a manually digitized glacier boundary for extracting the glacier area to map glacier facies within it, and does not consider separation of SGD from surrounding terrain. However, most of these studies either have ambitious data and processing requirements, complex procedural steps or have transferability issues (Tiwari and others, in press), which limits repeated applicability.

Thus, there is still a need to devise a methodology that may prove more efficient and consistent in mapping various glacier terrain classes (snow-ice, vegetation, water, IMD, SGD, PGD and valley rock), leading towards automatic mapping of glacier boundaries. To this end, a hierarchical knowledge-based approach is proposed here for sequential differentiation of various glacier terrain classes, with particular emphasis on SGD, PGD and valley rock owing to their spectral similarity.

STUDY AREA

The current study is focused on Kolahoi Glacier and the adjoining areas (34°11′–34°21′N, 75°27′–75°39′E), located in Lidder valley, western Himalaya (Fig. 1). The meltwater stream of Kolahoi Glacier is known as the West Lidder River and joins the East Lidder River at Pahalgam (35 km from the snout). Pahalgam is connected to Srinagar by road and from there to Aru (i.e. first 11 km). Beyond that, the remaining 24 km to the glacier snout have to be covered either on foot or by pony (Ahmad and Hashmi, 1974). The glacier is ∼5 km long and has an area of ∼11 km². Its headwall is located at 5425 m a.s.l. on Kolahoi mountain, between the peaks of Dudnag in the west and Hiurbagwan in the east (Kaul, 1990). The glacier surface is marked by crevasses along the eastern margins of the ablation zone and an extensive mass of debris along the western margin (Kaul, 1990).

Records of previous visits to, and studies on, Kolahoi Glacier suggest that the focus was mainly on field mapping (Neve, 1910), estimates of retreat (Neve, 1910; Odell, 1963; Kaul, 1990; Kanth and others, 2011), geomorphology and palaeoglaciation (Ahmad and Hashimi, 1974; Kaul, 1990) of the glacier. However, to date, there has been no study reported on differentiation of glacier facies and boundary mapping of Kolahoi Glacier.

DATA AND METHODOLOGY

Dataset used

Advanced Spaceborne Thermal Emission and Reflection Radiometer (ASTER) data acquired on 20 September 2003 were selected as the primary dataset, on the basis of minimal

Table 1. Description of the spectral indices discussed in this study. Formulation subscripts indicate ASTER band numbers

Spectral index	Source	Formulation	Utility
Normalized-difference snow index (NDSI)	Dozier (1989)	$NDSI = \dfrac{Green_{(ast\_b1)} - SWIR_{(ast\_b5)}}{Green_{(ast\_b1)} + SWIR_{(ast\_b5)}}$	Mapping and differentiating between snow-ice covered areas and non-snow-and-ice areas
Normalized-difference debris index (NDDI)	This study	$NDDI = \dfrac{SWIR_{(ast\_b6)} - -TIR_{(ast\_b14)}}{SWIR_{(ast\_b6)} + TIR_{(ast\_b14)}}$	Mapping and differentiating between supra-glacial debris and that of the terrain
Normalized-difference water index (NDWI)	McFeeters (1996)	$NDWI = \dfrac{Green_{(ast\_b1)} - -NIR_{(ast\_b3)}}{Green_{(ast\_b1)} + NIR_{(ast\_b3)}}$	Mapping surface water
Normalized-difference glacier index (NDGI)	Keshri and others (2009)	$NDGI = \dfrac{Green_{(ast\_b1)} - -Red_{(ast\_b2)}}{Green_{(ast\_b1)} + Red_{(ast\_b2)}}$	Mapping and differentiating between snow-ice and ice-mixed debris class

cloud cover, good contrast between various land covers and suitable acquisition date (ablation season). The scene was devoid of seasonal snow cover. Two ASTER data products, namely AST14DMO (registered at sensor L1B) and AST08 (surface kinetic temperature), were downloaded free of charge from NASA's Earth Observing System Data and Information System (https://reverb.echo.nasa.gov), under the auspices of the Global Land Ice Measurements from Space (GLIMS) project. The ASTER Global Digital Elevation Model (ASTER GDEM v2), which is freely available, was also downloaded from the US Geological Survey (USGS) website (http://glovis.usgs.gov/). Additionally, 42 field-based observations were collected during September 2014, using a handheld Trimble GPS (Fig. 1). Such GPS devices provide horizontal accuracy of up to ±3.9 m and vertical accuracy of ±15 m in mountainous terrain (Racoviteanu and others, 2007; Bhardwaj and others, 2015). The comparison of z-coordinates of the field points and corresponding elevations of the GDEM showed a mean difference and standard deviation of –33 m and 23 m, which we take as the offset and uncertainty, respectively. Information regarding the glacier terrain classes (vegetation, water, PGD, SGD and valley rock) present at these measurement points was recorded and later used to assess the positional accuracy of the glacier terrain classes mapped using hierarchical knowledge-based classification (HKBC).

Implementation of HKBC

Mapping of various glacier terrain classes (snow-ice, vegetation, water, IMD, SGD, PGD and valley rock) using HKBC involves several steps, namely data preprocessing, derivation of the knowledge base and hierarchical classification of glacier terrain classes, which are described below.

Preprocessing of data

Preprocessing involved the conversion of visible near-infrared (VNIR) and shortwave infrared (SWIR) data to reflectance, and thermal data to brightness temperature. Optical data were first converted to radiance, then radiometric (atmospheric and topographic) corrections were applied to retrieve reflectance values. Details of these procedures are provided by Shukla and others (2010a). It is pertinent to mention that coefficients of determination obtained by regression between corrected reflectance and terrain illumination were found to be near zero ($r^2 = \sim 0.005$), suggesting minimal effect of topography. Atmospherically corrected radiances of thermal infrared (TIR) bands were converted to brightness temperatures (K) using Planck's radiation equation (Yin and others, 2013). Finally, ASTER SWIR, thermal bands and GDEM were resampled to 15 m by

nearest-neighbour interpolation in order to match the spatial resolution of the visible bands for band ratio computations.

Derivation of the knowledge base

The approach proposed here requires several input layers: NIR/SWIR ratio and spectral indices (normalized-difference glacier index (NDGI), normalized-difference water index (NDWI), normalized-difference debris index (NDDI)) (Table 1), image transformations (intensity hue saturation (IHS) image), topographic attributes (slope) and the thermal glacier mask (TGM). The various processing steps involved in generating these input layers are discussed next.

The NIR/SWIR ratio image (Fig. 2a) and NDGI (Keshri and others, 2009) were obtained from multispectral ASTER data for mapping of snow-ice and IMD. The normalized-difference snow index (NDSI) was also tested, but not used here as it misclassified water bodies as snow-ice, probably because of their similar bulk optical properties in the VNIR (Dozier, 1989). The NDWI (Fig. 2b) was derived from ASTER1 and ASTER3 bands and facilitated the delineation of water (McFeeters, 1996). Many previous studies have applied band ratio algorithms for mapping of snow-ice, IMD and water, with satisfactory results (Paul and others, 2004; Bolch and Kamp, 2006; Keshri and others, 2009; Racoviteanu and Williams, 2012).

Nevertheless, the main challenge in the current study was to differentiate and map PGD and SGD. To achieve their differentiation, two new input layers (TGM and NDDI) were generated which depend upon the optical and thermal characteristics of these classes (Fig. 3a and b). Past remote-sensing studies have revealed that there exists considerable temperature difference between SGD and PGD cover classes (Taschner and Ranzi, 2002; Ranzi and others, 2004; Shukla and others, 2010a), probably due to glacial ice present beneath the SGD. This has been used by some workers as a source of additional information for segregation of PGD and SGD (Shukla and others, 2010a; Casey and others, 2012). Using this preliminary idea, an in-depth investigation of surface temperatures was carried out and it was observed that the surface temperature of glacier cover classes (snow-ice, IMD and SGD) does not exceed 283 K. Therefore, this criterion has been applied here for generation of a TGM, separating the classes with temperature below 283 K as glacier cover classes (snow-ice, IMD and SGD), from the classes with temperature above 283 K as non-glacier cover classes (PGD, vegetation, water and valley rock) (Fig. 2c). The TGM so obtained is a binary map (TGM = 0 for non-glacier area and TGM = 1 for glacier area; Fig. 2c). The temperatures of the non-glacier cover classes in the shadowed regions were found to exceed those of glacier
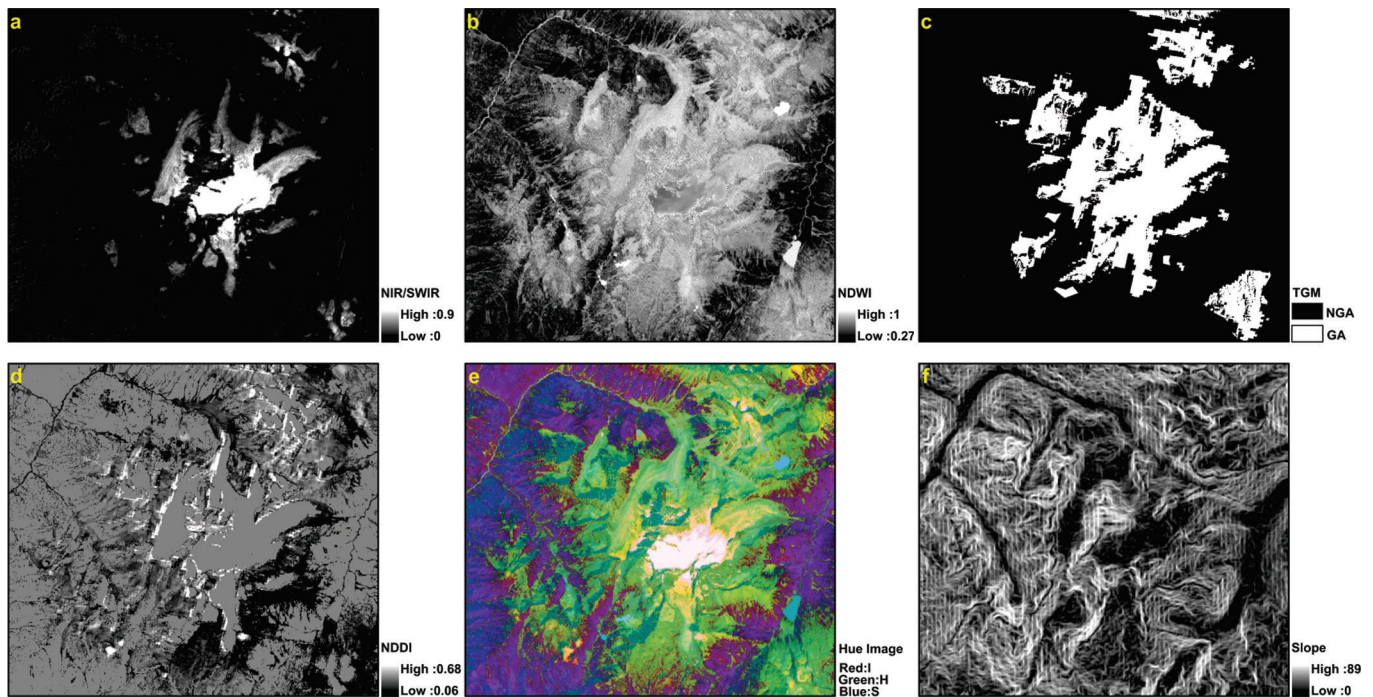
Fig. 2. The main input layers used in the hierarchical knowledge-based classifier: (a) NIR/SWIR (values 0–0.9); (b) normalized difference water index (values 0.27–1); (c); thermal glacier mask (TGM) (NGA: non-glacier area, GA: glacier area); (d) normalized-difference debris index (NDDI) (values 0.06–0.68); (e) hue image (values 0.074–1); and (f) slope map (values 0–89).

cover classes. This is in agreement with the results obtained by Shukla and others (2010b) and Karimi and others (2012).

Observing the spectral curves of SGD vis-à-vis other classes, it was noticed that SGD showed higher response in the SWIR region (ASTER band 6), similar to PGD and valley rock (Fig. 3a and b), because the three are compositionally the same. However, the response of supraglacial debris deviates considerably from the other two classes (PGD and valley rock) in the TIR region (ASTER band 14). This is because SGD has lower temperature than PGD and valley rock (Taschner and Ranzi, 2002; Ranzi and others, 2004)

due to the underlying glacier ice. The contrasting spectral response of these classes was used to formulate a new index, the NDDI. The SWIR and TIR bands were normalized before creation of NDDI in order to resolve the dimensional conflict. This index highlights the supraglacial debris in the region (Fig. 2d). The formulation of the index is given in Table 1. Thus, both TGM and NDDI were employed to separate SGD from PGD and valley rock.

ASTER bands 1–3 were transformed to intensity–hue–saturation (IHS) space (Fig. 2e). The hue component highlighted the vegetated area (purple) and thus facilitated the
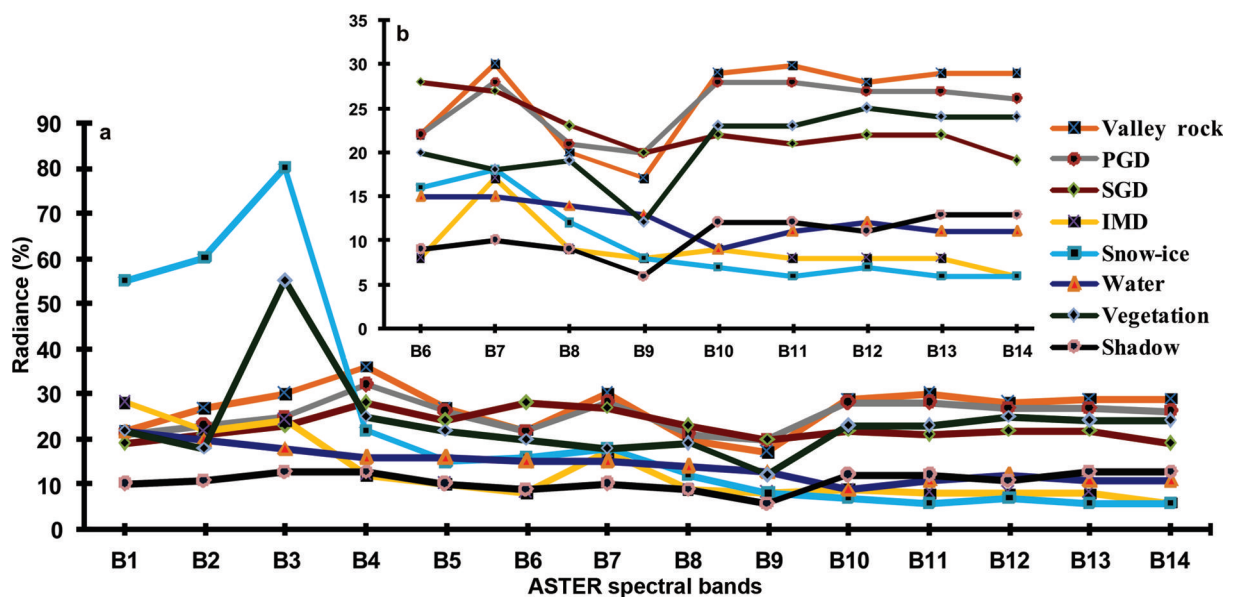
Fig. 3. (a) Spectral response curves derived from ASTER image; (b) zoomed-in view of spectral response curve from B6 to B14. Coloured lines represent the spectral behaviour of various classes. The *x*-axis represents different ASTER spectral bands (B1–B14). The *y*-axis denotes percentage spectral radiance. PGD: periglacial debris; SGD: supraglacial debris; IMD: ice-mixed debris.
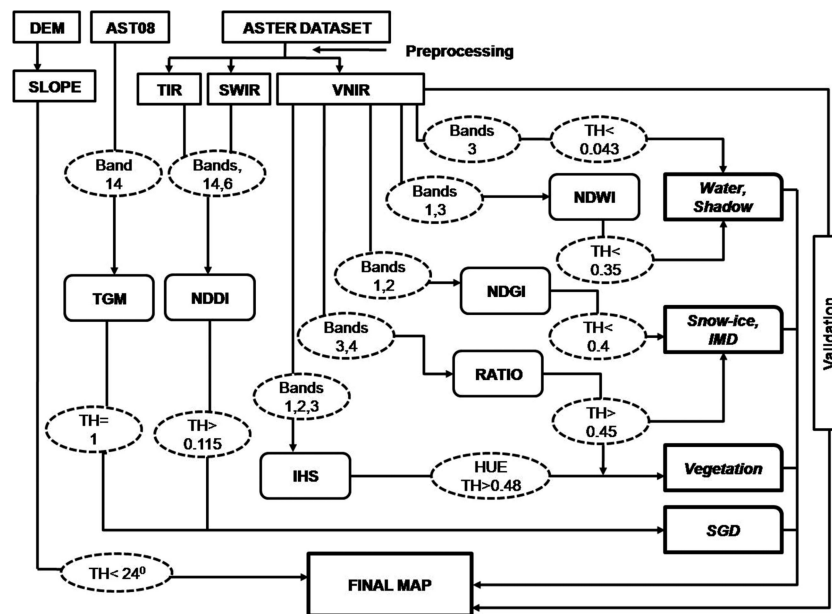
Fig. 4. Conceptual flow chart of the HKBC scheme for glacier terrain mapping. TH: threshold; NDWI: normalized-difference water index; NDGI: normalized-difference glacier index; IHS: intensity hue saturation; TGM: thermal glacier mask; NDDI: normalized-difference debris index; IMD: ice-mixed debris; SGD: supraglacial debris. Final Map constitutes shadow, water, snow-ice, IMD, vegetation, SGD, periglacial debris and valley rock.

extraction of vegetation (Fig. 2e). Paul and others (2004) and Racoviteanu and Williams (2012) have previously used the IHS transformation to map vegetation and bare rock. A slope map (Fig. 2f) derived from the ASTER GDEM facilitated the separation of PGD and valley rock. DEM-derived attributes (slope, aspect and curvature) have been used for glacier terrain mapping in previous studies (Paul and others, 2004; Bolch and others, 2010; Racoviteanu and Williams, 2012).

Hierarchical classification of glacier terrain classes

Under this heading, we describe the individual steps followed in HKBC for mapping different glacier terrain classes. The processing workflow is schematically shown in Figure 4.

(a) Shadow and water

Before mapping any glacier terrain class, the shadowed regions were automatically delineated using ASTER band 3, and a threshold value of 0.043 (band 3 < 0.043 = shadow) was applied (Fig. 4). This helped to reduce misclassifications among glacier terrain classes. Racoviteanu and Williams (2012) adopted a similar approach to remove shadowed regions. In the same step, water was differentiated by NDWI, applying a threshold of 0.35 (NDWI < 0.35 = water). The shadowed areas are shown in black, and water as blue, in Figure 5a.

(b) Snow-ice and IMD

Both snow-ice and IMD were mapped using the NIR/SWIR ratio image and NDGI. A threshold value of 0.45 (NIR/SWIR > 0.45 = snow-ice) was found to be suitable for snow-ice, and for IMD a threshold of 0.4 (NDGI < 0.4 = IMD) was found to be satisfactory (Figs 4 and 5b). Snow was more prevalent than ice, but the classification does not distinguish between them.

(c) Vegetation

The hue and NIR/SWIR images were found to be useful for mapping vegetation with a threshold of 0.48 and 0.45, respectively (Hue > 0.48 and NIR/SWIR > 0.45 = vegetation) (Figs 4 and 5c). Caution was exercised in selecting this threshold as it is known that sparse vegetation can grow on debris-covered parts of glaciers during spring (Bolch and others, 2007).

(d) Supraglacial debris

TGM and NDDI were used to map the SGD in the area, by employing a threshold of 0.115 (TGM = 1 or NDDI > 0.115 = SGD) (Figs 4 and 5d). TGM was able to classify those regions as SGD where NDDI could not map it and vice versa.

(e) Periglacial debris and valley rock

In-depth analysis of the slope values showed that the debris-covered regions had a slope range of 0–24°. A maximum value of 24° (slope < 24° = PGD, else valley rock) was selected to map PGD in agreement with previous studies (Paul and others, 2004; Karimi and others, 2012), which suggest that most of the debris-covered regions can be captured at this slope threshold since debris tends to rest on gentler slopes (Fig. 4). This step resulted in the final glacier terrain map, showing PGD (grey) and valley rock (tan) in addition to the other glacier terrain classes discussed above (Fig. 6a).

Once the glacier terrain classes have been mapped, the glacier boundary can be delineated by merging the glacier cover (i.e. snow-ice, IMD and SGD) and non-glacier cover (i.e. PGD, valley rock, water, shadow and vegetation) classes (Shukla and others, 2010a).

RESULTS AND DISCUSSION

The efficiency of the proposed HKBC approach for mapping various glacier terrain classes was tested by a two-way accuracy assessment process. First, the accuracy of the glacier terrain maps obtained via HKBC and MLC was assessed against the reference image (ASTER VNIR). Secondly, the boundary of the glacier delineated using the glacier terrain map was evaluated against the manually digitized boundary of the glacier (by visual interpretation of the ASTER VNIR image).
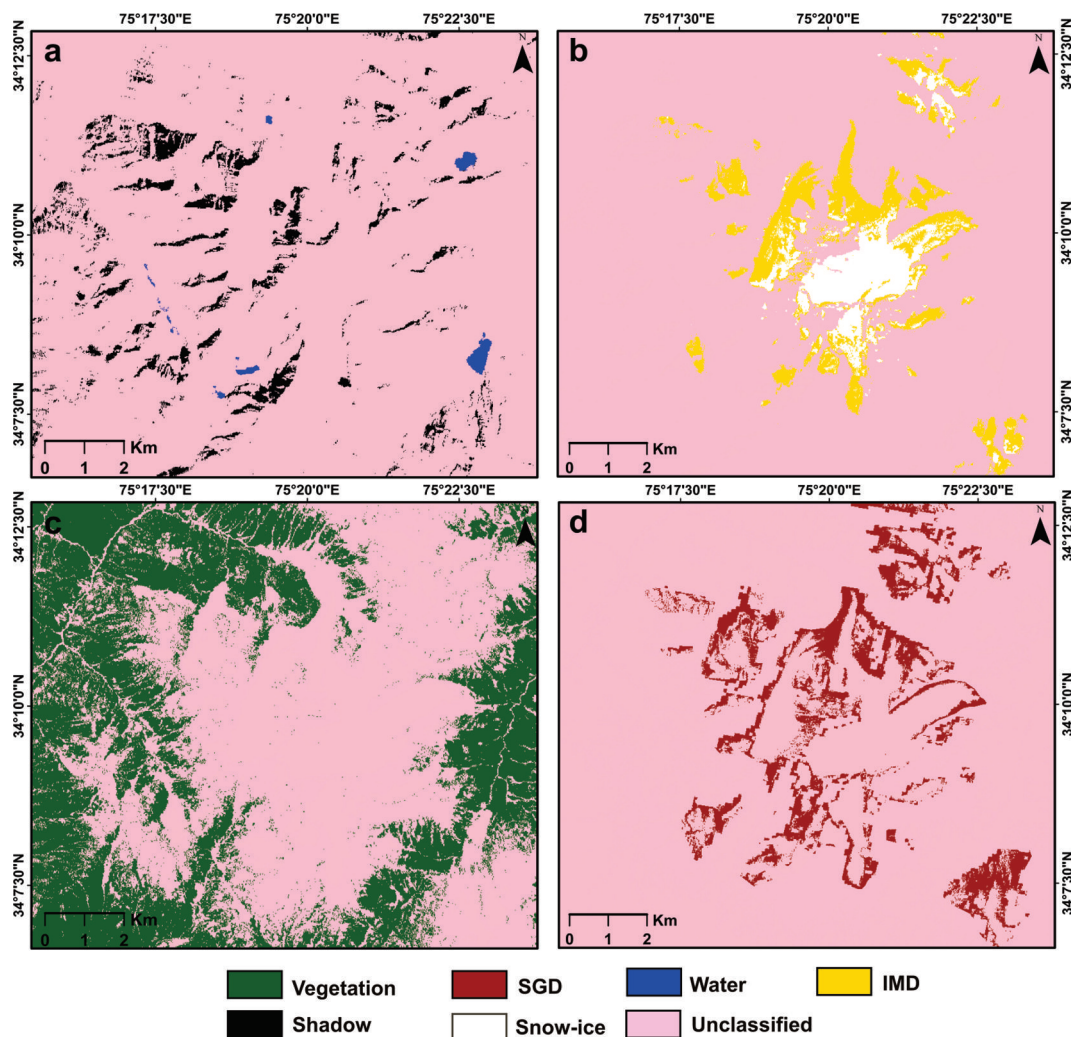
Fig. 5. Six of the classes obtained through HKBC: (a) shadowed areas in black, and water in blue; (b) snow-ice in white, and gold pertaining to ice-mixed debris; (c) vegetation in green; (d) SGD in brown. SGD: supraglacial debris; IMD: ice-mixed debris.

Accuracy of glacier terrain mapping

The final glacier terrain map obtained from HKBC was validated against the ASTER VNIR image (15 m spatial resolution) and 42 field-based observations. The ASTER VNIR image was considered as reference because there was no higher-resolution image available for this date. To determine the efficacy of HKBC, conventional-error-matrix based measures, namely overall user's and producer's accuracy (Foody, 2002), were determined (Table 2). The overall accuracy (OA) is used to indicate the accuracy of the whole classification (i.e. number of correctly classified pixels divided by total number of testing pixels). OA does not take into account the off-diagonal elements of the error matrix which represent the misclassification errors, i.e. errors of omission and commission. However, the kappa coefficient does take these errors into account, and is thus considered a better estimate of classification accuracy. Corresponding to these errors, a new set of accuracy measures may be derived: producer's accuracy (PA) and user's accuracy (UA). The PA relates to the probability that a reference sample is correctly mapped and measures the error of omission. The UA indicates the probability that a sample from the classified map actually matches what it is in the reference data and measures the commission error. High individual accuracies with minimal difference between them indicate accurate differentiation of the concerned class.

A testing dataset constituting 650 pixels was taken using stratified random sampling, and additionally 42 ground control points (692 points in total) were taken for evaluating the accuracy of various glacier terrain classes. Reference

Table 2. User's accuracy (UA) and producer's accuracy (PA) of individual glacier terrain classes derived from HKBC and maximum likelihood classifier (MLC). The overall accuracy produced by HKBC is 89%, and a kappa coefficient of 0.86 and MLC resulted in an overall accuracy of 63% with a kappa coefficient of 0.60

Class name	HKBC		MLC	
	UA%	PA%	UA%	PA%
Snow-ice	91	94	89	83
IMD	91	85	62	70
SGD	81	88	41	46
PGD	78	81	36	35
Valley rock	87	80	49	45
Vegetation	95	100	91	92
Water	88	93	69	85
Shadow	89	83	53	48

Fig. 6. Comparison of the glacier terrain mapping from the proposed HKBC and supervised classification (MLC). (a) Final map obtained from HKBC scheme; (b) map obtained from MLC. The rectangles in (a) and (b) are enlarged in (c) and (d) respectively. SGD: supraglacial debris; IMD: ice-mixed debris; PGD: periglacial debris.

classes for all the testing pixels were derived on the basis of visual image interpretation of the reference image with special consideration of their respective spectral curves (Fig. 3a and b). The accuracy of the present classification was reduced after inclusion of the field reference points in the testing dataset. This may be attributed to the considerable time gap between image acquisition (2003) and field survey (2014) as well as to the limited accuracy of the GPS observations. Lacking any other reliable data for validation, these observations on relatively stable land covers were accepted as valid. Further, the results from HKBC were also compared with a supervised classification, performed on the same dataset using a maximum likelihood classifier (MLC) (Richards and Jia, 1999). MLC is known to have serious limitations in processing data from multiple sources, as it requires the data to follow normal distributions (Watanacha-turaporn and others, 2008). Nonetheless, it remains the most widely used classifier for glacier terrain mapping (Karimi and others, 2012; Khan and others, 2015; Tiwari and others, in press). Thus, a critical assessment of the relative utility of the two classifiers for glacier terrain mapping is pertinent to encourage the future use of HKBC, instead of MLC.

The classification generated from HKBC showed an overall accuracy of 89% and kappa coefficient of 0.86,

whereas MLC yielded an overall accuracy of 63% with a kappa coefficient of 0.60. Table 2 shows the individual class accuracies, i.e. UA and PA, of various glacier terrain classes obtained from the two classifiers. The accuracy with which the glacier cover and non-glacier cover were mapped is discussed next.

Glacier cover classes
The glacier cover classes are snow-ice, IMD and SGD. HKBC achieved high UA and PA in the range 85–94% for mapping of snow-ice and IMD (Table 2). However, the difference between the two accuracies was lower for snow-ice (3%) than for IMD (6%), which may be attributed to the spectrally mixed nature of IMD. Although MLC yielded comparable results to HKBC in mapping snow-ice, it misclassified parts of snow-ice as IMD, evident through visual inspection of the ASTER image (Fig. 1; black arrow in Fig. 6a). These differences in the classification accuracy results arose by misclassification of IMD into snow-ice and SGD.

Identification and mapping of SGD is critical due to its spectral similarity with PGD and valley rock. The novel approach used here in HKBC successfully mapped SGD with high accuracy (UA = 81%, PA = 88%). The 7% differ-ence here between UA and PA may be linked to

Manual boundary ━━━━━ HKBC boundary ━━━━━ MLC boundary ━━━━━
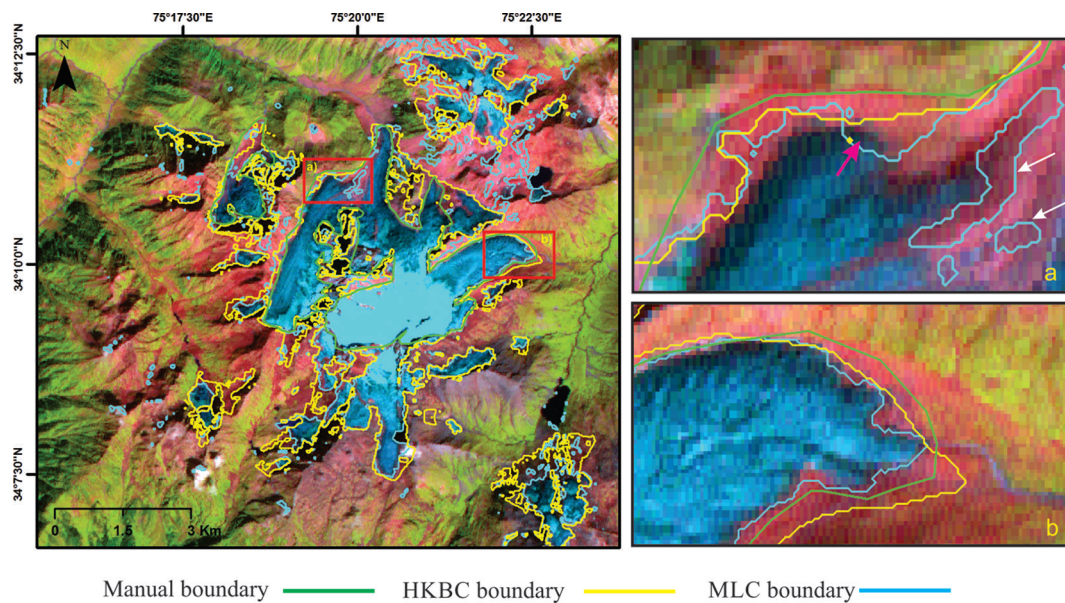
Fig. 7. Comparison of the glacier boundary derived from the present approach with the MLC boundary and the manual interpretation. (a) Delineation of the boundary where glacier margin is heavily debris-covered. White arrows show SGD areas misclassified as PGD by MLC and hence excluded from glacier area. Pink arrow shows exclusion of IMD from glacier area by MLC-derived boundary. (b) Glacier boundary mapping at the secondary snout of Kolahoi Glacier. Note that while MLC boundary follows the edge of exposed ice and manual boundary relies on debris hues, the HKBC boundary follows the edge of ice extensions beneath debris cover. (ASTER false-color composite with band combination R = SWIR, G = NIR and B = red band is displayed as background.)

misclassification as SGD of some pixels scattered into the TGM, owing to their lower temperatures (<283 K). MLC was poor at classifying SGD (UA = 41%, PA = 46%). This fact is well established from the spatial disposition of this class in the glacier terrain map (Fig. 6c and d) as well as the individual accuracy values of these classes (Table 2). Lower individual accuracies of SGD clearly show the inability of MLC to handle the inherent spectral variability of this class.

Non-glacier cover classes

The non-glacier cover classes include vegetation, water, shadow, PGD and valley rock. Results from HKBC for mapping of vegetation, water and shadow showed that it performed well (Table 2; Fig. 6c and d). Both UA and PA exceed 83%, and a difference of not more than 6% is found in these cases (Table 2). This connotes accurate mapping and minimal misclassification among these classes, which is probably a result of distinct mapping methodologies adopted in HKBC while segregating each of these classes. While MLC achieved comparable results for vegetation, its mapping of water and shadowed regions was unsatisfactory (Table 2). Most of the shadowed regions in MLC were misclassified as valley rock and PGD (red arrows in Fig. 6b).

Separation and precise mapping of PGD was again a crucial step as far as non-glacier cover classes were concerned. PGD exhibited the lowest values of both accuracies (UA = 78% and PA = 81%) relative to other classes (Table 2). This is probably due to the application of fixed thresholds for separating PGD from SGD and valley rock. The misclassification of PGD as valley rock is also evident from the glacier terrain maps (blue arrow in Fig. 6b) and can be mainly accredited to the constant criterion of slope (slope > 24° = valley rock, else PGD) applied for its differentiation. In particular, this slope threshold may not be appropriate for some parts within the scene. Despite this, the importance of slope among other topographic attributes in

glacier terrain mapping has been emphasized by several previous studies (Paul and others, 2004; Bolch and Kamp, 2006; Shukla and others, 2010a; Racoviteanu and Williams, 2012; Rastner and others, 2014). Similarly, the constant temperature criterion (<283 K) applied for separation of SGD and PGD may not be applicable to some parts of the scene where it resulted in mutual misclassifications. Detailed analysis of these layers and application of variable thresholds (sector-wise) needs to be further investigated. MLC performs poorly in mapping PGD (Table 2). Figure 6c and d focus on comparative misclassification of SGD and PGD, which is more pronounced in MLC than HKBC. Again, HKBC mapped valley rock comprehensively with accuracy values of UA = 87%, PA = 80%, but MLC accuracies were lower (UA = 49%, PA = 45%). The lower mapping accuracy of MLC can be ascribed to the spectral similarity of PGD, SGD and valley rock (Fig. 3a and b).

A Z-test at the 95% confidence level was performed on classification results. In summary, HKBC has proved to be a more consistent classifier for glacier terrain mapping, especially with reference to spectrally similar classes (SGD, PGD and valley rock) which usually limit the accurate mapping of glaciers.

Glacier boundary

Here we evaluate the glacier boundary obtained from HKBC by comparing it with those derived from MLC and manual digitization. Comparing these boundaries, it is found that HKBC maps the glacier boundary most accurately where it is concealed by debris cover (Fig. 7a and b). While the boundary delineated by visual interpretation relies mostly on the optical properties of the debris cover (pinkish red hue in Fig. 7a and b), that from HKBC utilizes information from SWIR and thermal data to map the extent of debris-covered ice. The MLC boundary shows gross errors. It may either follow the edge of the exposed ice (Fig. 7b) or even exclude

some of it when mixed with debris cover (pink arrow in Fig. 7a). MLC misclassified some SGD as PGD (white arrows in Fig. 7a), resulting in elimination of some glacier area. However, the boundary derived from HKBC neither simply follows the ice margins nor depends solely on the optical spectral properties of debris cover. It maps the glacier boundary including the hidden ice beneath the debris cover.

Sources of uncertainty, limitations and scope of refinement

Possible sources of uncertainty in mapping glacier terrain classes include positional, preprocessing, data quality, interpretative and conceptual errors (Racovitaneau and Williams, 2012; Paul and others, 2013). The positional error of various glacier-terrain class boundaries mapped by HKBC was quantified by estimation of error-matrix based accuracy measures, taking the ASTER VNIR image and 42 field points as reference. These accuracy values were within the acceptable value of 85% suggested in the USGS classification scheme (Foody, 2002). The availability of a higher-resolution reference dataset would have resulted in better retrospective appraisal of the results. The lower values of the coefficient of determination obtained by regression of reflectance against illumination of the terrain ($\cos i$) prove the reliability of the preprocessing techniques applied here. Moreover, the error involved in the elevation data was also quantified by using the altitude points collected in the field. The interpretation and conceptual errors, which may constitute prime sources of uncertainty, also appear to be within acceptable limits (Table 2).

At this stage, it is also important to evaluate the limitations of the approach when applied over an extended area, which should be taken as a continuation of this study. As HKBC involves the application of various thresholds, these may vary when the approach is applied elsewhere. For example, mapping PGD and valley rock in the proposed approach relies on a slope threshold, which may differ with variation in topography and glacier type (Bolch and Kamp, 2006; Rastner and others, 2014). Also, the differentiation of SGD from other classes relies on thermal data, and thresholds that depend upon variations in the local temperature regime may drastically change. The solution to this may be to conduct a thorough sensitivity analysis to explore the possibility of standardizing the thresholds. A sensitivity analysis would be required primarily to assess the impact of changing thresholds on segregation of different glacier classes. Additionally, delineation of glacier terrain classes in shadowed regions remains a bottleneck. The potential of thermal and slope information revealed by the present study suggests that better spatial resolution of these properties would definitely enhance the precision of glacier terrain mapping. Furthermore, it would be interesting to explore the SWIR bands of Landsat 8 for application of this approach in the absence of these bands in newer ASTER datasets.

SUMMARY AND CONCLUSIONS

In this study, a hierarchical knowledge-based classifier was proposed for mapping various glacier terrain classes. The classifier discerned snow-ice, water, IMD and vegetation by employing NIR/SWIR, NDWI, NDGI and hue, respectively. The spectral response ratios and temperature analysis of spectrally similar classes (PGD, SGD and valley rock) differed noticeably. Hence, this idea was employed to generate TGM and NDDI, which along with slope were used for their differentiation. The HKBC results were tested against the ASTER VNIR image and 42 field reference points. HKBC was successful in classifying all eight glacier terrain classes mapped here, with an overall accuracy of 89%. UA and PA of all the classes were within acceptable limits, except for PGD which showed relatively lower values. The study also compared the HKBC results with those obtained from MLC, which misclassified the spectrally similar classes (PGD, SGD and valley rock). The significance of HKBC results relative to those from MLC was also corroborated through a Z-test. Similarly, the glacier boundary derived from HKBC proved to be more appropriate when compared with those obtained from MLC and visual interpretation, as it was capable of delineating debris-covered ice by incorporating thermal information. Future work should be focused on eliminating the limitations of the present study and enhancing its robustness, particularly by sensitivity analysis to explore the possibility of standardizing the various thresholds applied in the approach. Transferability of the methodology presented here to some other area, in its absolute form, would necessitate thorough understanding of the datasets, study area and basis behind each condition applied for sequential retrieval of various classes. Moreover, the thresholds applied to derive the final results may vary with scene and study area although the rationale behind the outlined steps would remain the same. Also, the mapping accuracy can be greatly enhanced by improving the spatial resolution of the thermal bands and DEMs.

From the outcomes of this study, it can be concluded that this approach may prove effective in mapping glacier terrain classes, especially where glaciers are accompanied by varying amounts of debris in their ablation areas, which is a persistent challenge.

REFERENCES

Ahmad N and Hashimi NH (1974) Glacial history of Kolahoi Glacier, India. *Int. J. Glaciol.*, **13**(68), 279–283

Bayr KJ, Hall DK and Kovalick WM (1994) Observation on glaciers in the Eastern Austria Alps using satellite data. *Int. J. Remote Sens.*, **15**, 1733–1742

Bhambri R, Bolch T and Chaujar RK (2011) Mapping of debris-covered glaciers in the Garhwal Himalayas using ASTER DEMs and thermal data. *Int. J. Remote Sens.*, **32**, 8095–8119

Bhambri R, Bolch T and Chaujar RK (2012) Frontal recession of Gangotri Glacier, Garhwal Himalayas, from 1965 to 2006, measured through high resolution remote sensing data. *Current Sci.*, **102**(3), 489–494

Bhardwaj A, Joshi PK, Snehmani SL, Singh MK, Singh S and Kumar R (2015) Applicability of Landsat 8 data for characterizing glacier facies and supraglacial debris. *Int. J. Appl. Earth Obs. Geoinf.*, **38**, 51–64

Bolch T and Kamp U (2006) Glacier mapping in high mountains using DEMs, Landsat and ASTER data. *Grazer Schr. Geogr. Raumforsch.*, **41**, 13–24

Bolch T, Buchroithner, MF Kunert A and Kamp U (2007) Automated delineation of debris-covered glaciers based on ASTER data. In Gomarasca, MA ed. *GeoInformation in Europe. Proceedings of the 27th EARSeL Symposium, 4–6 June 2007, Bolzano, Italy.* Millpress, Rotterdam, 403–410

Bolch T, Buchroithner M, Pieczonka T and Kunert A (2008) Planimetric and volumetric glacier changes in the Khumbu Himal, Nepal, since 1962 using Corona, Landsat TM and ASTER data. *J. Glaciol.*, **54**(187), 592–600

Bolch T, Menounos B and Wheate R (2010) Landsat-based glacier inventory of western Canada, 1985–2005. *Remote Sens. Environ.*, **114**, 127–137 (doi: 10.1016/j.rse.2009.08.015)

Burns P and Nolin A (2014) Using atmospherically-corrected Landsat imagery to measure glacier area change in the Cordillera Blanca, Peru from 1987 to 2010. *Remote Sens. Environ.*, **140**, 165–178 (doi: 10.1016/j.rse.2013.08.026)

Casey KA, Kääb A and Benn DI (2012) Geochemical characterization of supraglacial debris via in situ and optical remote sensing methods: a case study in Khumbu Himalaya, Nepal. *Cryosphere*, **6,** 85–100 (doi: 10.5194/tc-6–85-2012)

Dozier J (1989) Spectral signature of alpine snow-cover from the Landsat Thematic Mapper. *Remote Sens. Environ.*, **28**, 9–22

Foody GM (2002) Status of land cover classification accuracy assessment. *Remote Sens. Environ.*, **80**, 185–201

Jansson P, Hock R and Schneider T (2003) The concept of glacier storage: a review. *J. Hydrol.*, **282**(1–4), 116–129 (doi: 10.1016/S0022-1694(03)00258-0)

Kääb A (2002) Monitoring high-mountain terrain deformation from air- and spaceborne optical data: examples using digital aerial imagery and ASTER data. *ISPRS J. Photogramm. Remote Sens.*, **57**(1–2), 39–52 (doi: 10.1016/S0924-2716(02)00114-4)

Kanth TA, Shah AA and Hassan ZU (2011) Geomorphologic character and receding trend of Kolahoi Glacier in Kashmir Himalaya. *Recent. Res. Sci. Technol.*, **3**(9), 68–73

Karimi N, Farokhnia A, Karimi L, Eftekhari M and Ghalkhani H (2012) Combining optical and thermal remote sensing data for mapping debris-covered glaciers (Alamkouh Glaciers, Iran). *Cold Reg. Sci. Technol.*, **71**, 73–83 (doi: 10.1016/j.coldregions.2011.10.004)

Kaul MN (1990) *Glacial and fluvial geomorphology of Western Himalayas*. Concept Publishing Company, New Delhi

Keshri AK, Shukla A and Gupta RP (2009) ASTER ratio indices for supraglacial terrain mapping. *Int. J. Remote Sens.*, **30**(2), 519–524 (doi: 10.1080/01431160802385459)

Khan A, Naz SB and Bowling LC (2015) Separating snow, clean and debris covered ice in Upper Indus Basin, Hindukush–Karakoram, using Landsat images between 1998 and 2002. *J. Hydrol.*, **521**, 46–64 (doi: 10.1016/j.jhydrol.2014.11.048)

McFeeters SK (1996) The use of the Normalized Difference Water Index (NDWI) in the delineation of open water features. *Int. J. Remote Sens.*, **17**(7), 1425–1432 (doi: 10.1080/01431169608948714)

Neve EF (1910) Mt. Kolahoi and its Northern Glacier. *Alp. J.*, **25**, 39–42

Odell NE (1963) The Kolahoi northern glacier, Kashmir. *J. Glaciol.*, **4**(35), 633–635

Paul F and Mölg (2014) Hasty retreat of glaciers in northern Patagonia from 1985 to 2011. *J. Glaciol.*, **60**(224), 1033–1043 (doi: 10.3189/2014JoG14J104)

Paul F, Huggel C and Kääb A (2004) Mapping of debris-covered glaciers using multispectral and DEM classification techniques. *Remote Sens. Environ.*, **89**, 510–518 (doi: 10.1016/j.rse.3003.11.007)

Paul F and 19 others (2013) On the accuracy of glacier outlines derived from remote-sensing data. *Ann. Glaciol.*, **54**(63), 171–182 (doi: 10.3189/2013AoG63A296)

Racoviteanu A and Williams MW (2012) Decision tree and texture analysis for mapping debris-covered glaciers in the Kangchenjunga area, Eastern Himalaya. *Remote Sens.*, **4**, 3078–3109 (doi: 10.3390/rs4103078)

Racoviteanu AE, Manley WF, Arnaud Y and Williams M (2007). Evaluating digital elevation models for glaciologic applications: an example from Nevado Coropuna, Peruvian Andes. *Global Planet. Change*, **59**, 110–125 (doi: 10.1016/j.gloplacha.2006.11.036)

Ranzi R, Grossi G, Iacovelli L and Taschner S (2004) Use of multispectral ASTER images for mapping debris-covered glaciers within the GLIMS project. In *IGARSS 2004, International Geoscience and Remote Sensing Symposium, 20–24 September 2004, Anchorage, Alaska, USA. Proceedings, Vol. 2.* Institute of Electrical and Electronics Engineers, Piscataway, NJ, 1144–1147

Rastner P, Bolch T and Notarnicola C (2014) A comparison of pixel- and object-based glacier classification with optical satellite images. *IEEE J. Selected Topics Appl. Earth. Obs. Remote Sens.*, **7**(3), 853–862 (doi: 10.1109/JSTARS.2013.2274668)

Reid TD and Brock BW (2014) Assessing ice-cliff backwasting and its contribution to total ablation of debris-covered Miage glacier, Mont Blanc massif, Italy. *J. Glaciol.*, **60**(219), 3–13 (doi: 10.3189/2014JoG13J045)

Richards JA and Jia XP (1999) *Remote sensing digital image analysis*. Springer-Verlag, Berlin

Scherler D, Bookhagen B and Strecker MR (2011) Spatially variable response of Himalayan glaciers to climate change affected by debris cover. *Lett. Nature Geosci.*, **4**, 156–159 (doi: 10.1038/ngeo1068)

Shukla A, Gupta RP and Arora MK (2009) Estimation of debris cover and its temporal variation using satellite sensor data: a case study in Chenab Basin, Himalaya. *J. Glaciol.*, **55**(191), 444–452

Shukla A, Arora MK and Gupta RP (2010a) Synergistic approach for mapping debris-covered glaciers using optical–thermal remote sensing data with inputs from geomorphometric parameters. *Remote Sens. Environ.*, **114**, 1378–1387 (doi: 10.1016/j.rse.2010.01.015)

Shukla A, Gupta RP and Arora MK (2010b) Delineation of debris-covered glacier boundaries using optical and thermal remote sensing data. *Remote Sens. Lett.*, **1**(1), 11–17 (doi: 10.1080/01431160903159316)

Taschner S and Ranzi R (2002) Comparing opportunities of Landsat-TM and ASTER data for monitoring a debris covered glacier in the Italian Alps within the GLIMS project. In *IGARSS 2002, International Geoscience and Remote Sensing Symposium, 24–28 June 2002, Toronto, Canada. Proceedings, Vol. 2.* Institute of Electrical and Electronics Engineers, Piscataway, NJ, 1044–1046

Tiwari RK, Arora MK and Gupta RP (in press) Comparison of maximum likelihood and knowledge-based classifications of debris cover of glaciers using ASTER optical–thermal imagery. *Remote Sens. Environ.* (doi: 10.1016/j.rse.2014.10.026)

Watanachaturaporn P, Arora, MK and Varshney PK (2008) Multi-source classification using support vector machines: an empirical comparison with decision tree and neural network classifiers. *Photogramm Eng. Remote Sens.*, **74**(2), 239–246

Yin D, Cao X, Chen X, Shao Y and Chen J (2013) Comparison of automatic thresholding methods for snow-cover mapping using Landsat TM imagery. *Int. J. Remote Sens.*, **34**(19), 6529–6538 (doi: 10.1080/01431161.2013.803631)